2018 *Biochemistry* **2010,** *49,* 2018–2030
DOI: 10.1021/bi902027z

BIOCHEMISTRY
including biophysical chemistry & molecular biology
Article

Contributions of the Histidine Side Chain and the N-Terminal α-Amino Group to the Binding Thermodynamics of Oligopeptides to Nucleic Acids as a Function of pH[†]

Jeff D. Ballin,*[,‡] James P. Prevas,[‡] Christina R. Ross,[‡] Eric A. Toth,[‡] Gerald M. Wilson,[‡] and M. Thomas Record, Jr.[§]

[‡]*Department of Biochemistry and Molecular Biology and Marlene and Stewart Greenebaum Cancer Center, University of Maryland School of Medicine, Baltimore, Maryland 21201, and* [§]*Departments of Chemistry and Biochemistry, University of Wisconsin—Madison, Madison, Wisconsin 53706*

Received November 25, 2009; Revised Manuscript Received January 26, 2010

ABSTRACT: Interactions of histidine with nucleic acid phosphates and histidine pK_a shifts make important contributions to many protein−nucleic acid binding processes. To characterize these phenomena in simplified systems, we quantified binding of a histidine-containing model peptide HWKK ($^+NH_3$-His-Trp-Lys-Lys-NH_2) and its lysine analogue KWKK ($^+NH_3$-Lys-Trp-Lys-Lys-NH_2) to a single-stranded RNA model, polyuridylate (polyU), by changes in tryptophan fluorescence as a function of salt concentration and pH. For both HWKK and KWKK, equilibrium binding constants, K_{obs}, and magnitudes of log−log salt derivatives, $SK_{obs} \equiv (\partial \log K_{obs}/\partial \log[Na^+])$, decreased with increasing pH in the manner expected for a titration curve model in which deprotonation of the histidine and α-amino groups weakens binding and reduces its salt-dependence. Fully protonated HWKK and KWKK exhibit the same K_{obs} and SK_{obs} within uncertainty, and these SK_{obs} values are consistent with limiting-law polyelectrolyte theory for +4 cationic oligopeptides binding to single-stranded nucleic acids. The pH-dependence of HWKK binding to polyU provides no evidence for pK_a shifts nor any requirement for histidine protonation, in stark contrast to the thermodynamics of coupled protonation often seen for these cationic residues in the context of native protein structure where histidine protonation satisfies specific interactions (e.g., salt-bridge formation) within highly complementary binding interfaces. The absence of pK_a shifts in our studies indicates that additional Coulombic interactions across the nonspecific-binding interface between RNA and protonated histidine or the α-amino group are not sufficient to promote proton uptake for these oligopeptides. We present our findings in the context of hydration models for specific vs nonspecific nucleic acid binding.

Nucleic acid binding proteins typically possess a higher density of positively charged amino acids in the DNA[1] or RNA binding interface relative to elsewhere on the protein surface (*1*, *2*). In a comparison of 75 protein−nucleic acid crystal structures, DNA phosphates participated in 60% of all protein−DNA hydrogen bonds (including salt bridges), of which 41% were salt bridges with lysine or arginine (*1*). A recent survey of 45 protein−RNA costructures found that 68% of hydrogen bond interactions to the phosphodiester backbone were through lysine and arginine residues, with donor−acceptor distances strongly clustered within 2.5−3.1 Å to make the most favorable (i.e., dehydrated) hydrogen bonds (*3*). The contributions of lysine (*4*−*11*) and arginine (*11*−*13*) to peptide−nucleic acid binding have been extensively characterized and demonstrate that Coulombic interactions between cationic protein residues and the polyanionic nucleic acid backbone significantly stabilize the protein−nucleic acid complex and cause binding affinity to increase strongly with decreasing salt concentration.

Histidine can also be cationic and often makes important contacts in the protein−nucleic acid interface, many of which are essential or conserved across species. For example, direct phosphate−histidine interactions are observed for *Escherichia coli* CAP via the minor groove adjacent to the site of DNA bending (*14*, *15*) in the NF-κB-DNA complex at the −1 position of the DNA recognition sequence (*16*) and for T7 DNA polymerase with the primer phosphate backbone (*17*). Figure 1 shows the conserved histidine−phosphodiester interactions in the cocrystal structures of rat glucocorticoid receptor (GR) with DNA (*18*) and of Vts1 (a homologue of Smaug in animals) with RNA (*19*). Mutational studies disrupting histidine−phosphate interactions impact binding and catalytic activity for T7 polymerase with DNA (*20*) and ribonuclease A with RNA (*21*). Overall, histidine is the seventh most prevalent natural amino acid at the protein−DNA interface (*1*). In amino acid distribution surveys of protein−DNA (*1*) and protein−RNA costructures (*22*), histidine exhibits respectively the sixth and fifth highest ratio of binding interface vs surface distributions. Analysis of 129 protein−DNA structures revealed that 65% of direct histidine−DNA hydrogen bonds were to the phosphate backbone (*23*).

[†]This work was supported by funding from National Institutes of Health grants R01 CA102428 (to G.M.W.) and partial support from the University of Wisconsin—Madison Graduate School.

*To whom correspondence should be addressed. Phone: (410) 706-8903. Fax: (410) 706-8297. E-mail: jball003@umaryland.edu. Address: Department of Biochemistry and Molecular Biology, University of Maryland, 108 North Greene Street, Baltimore MD 21201.

[1]Abbreviations: ss, single-stranded; dsDNA, double-stranded DNA; GR, glucocorticoid receptor; PNAI, protein−nucleic acid interactions; polyU, polyuridylic acid; AICc, second-order Akaike information criterion; EDTA, ethylenediaminetetraacetic acid; HEPES, 4-(2-hydroxyethyl)-1-piperazineethanesulfonic acid; LBD, ligand binding density; SAM, sterile α motif; lacR, lac repressor; *Pw*TBP, *Pyrococcus woesei* TATA-binding protein; E2C, human papillomavirus type 16 E2 protein; T-ag-obd, origin-binding domain of SV40 T antigen.

 Published on Web 01/28/2010

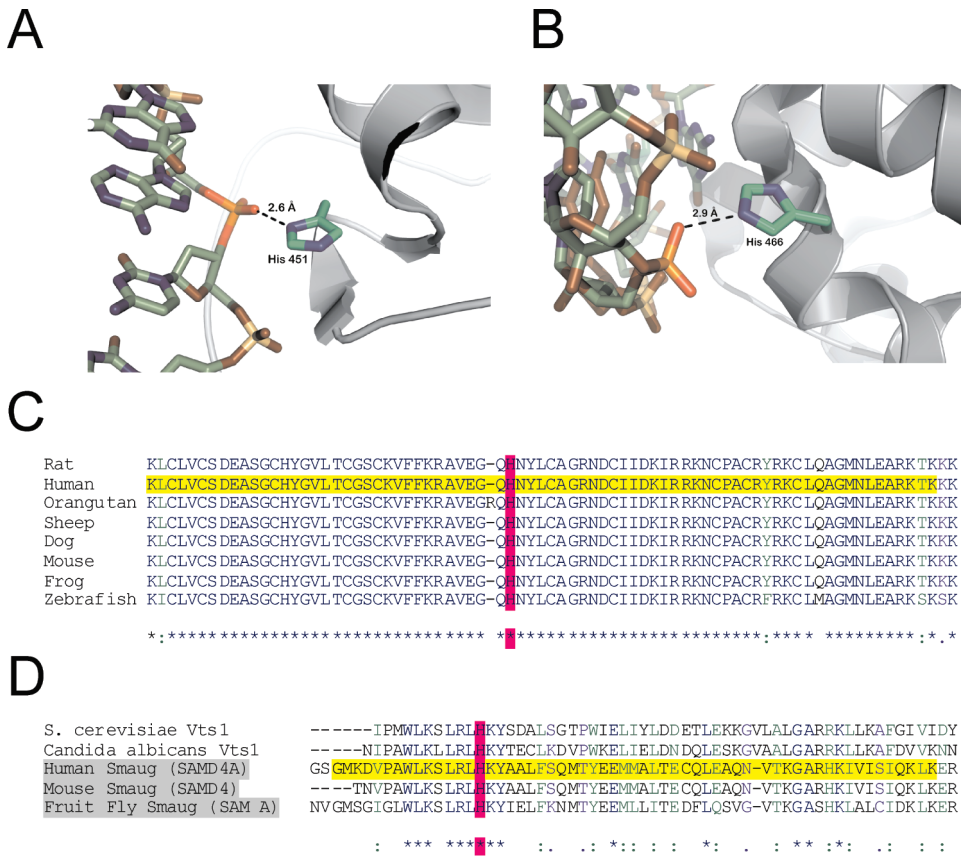

FIGURE 1: Representative crystal structures of conserved histidine−phosphodiester interactions. (A) The cocrystal of the rat glucocorticoid receptor DNA binding domain complexed with a glucocorticoid recognition element (pdb: 1R4R) (*18*). (B) A cocrystal of the SAM domain of the *Saccharomyces cerevisiae* post-transcriptional regulator Vts1p recognizing an RNA hairpin SAM recognition element (pdb: 2F8K) (*19*). (C) CLUSTALW analysis of a region within the glucocorticoid receptor DNA binding domain, highlighted in yellow. Database sequences were extracted from the following accession numbers: rat (*Rattus norvegicus*), NP_036708; human (*Homo sapiens*), CAJ65924; orangutan (*Pongo abelii*), NP_001126305; sheep (*Ovis aries*), NP_001107658; dog (*Canis familiaris*), ABA40754; mouse (*Mus musculus*), NP_032199; frog, NP_001081531; zebrafish (*Danio rerio*), NP_032199. (D) CLUSTALW analysis of the SAM RNA binding domain. Species highlighted in gray possess Smaug, a homologue of Vts1, which contains a conserved SAM domain highlighted yellow for the human sequence. Accession numbers used were *Saccharomyces cerevisiae*, NP_015004; *Candida albicans*, Q5AI80; human (*Homo sapiens*), NP_056404; mouse (*Mus musculus*), NP_083242; fruit fly (*Drosophila melanogaster*), NP_523987. In (C) and (D), the respective conserved histidines shown in panels (A) and (B) are highlighted in pink. The symbols below the sequence data in (C) and (D) denote CLUSTALW-defined sequence conservation: "*" indicates a fully conserved residue; ":", strongly conserved; ".", weakly conserved.

To our knowledge, no binding studies have been reported on histidine−nucleic acid model systems. Thermodynamic effects of histidine and other cationic residues on the thermal denaturation of DNA−oligopeptide conjugates have been reported (*24*), but data of this type only detect differences in interactions of the cationic residues with the native and denatured states of the nucleic acids. The frequency with which histidine is found in protein−nucleic acid interfaces suggests that histidine plays an important role in these binding processes. How does the behavior of histidine in a nonspecific ligand−nucleic acid complex compare to that seen for specific binding interactions such as those described above? What do these similarities and differences tell us? This study compares the nonspecific binding contributions of histidine vs lysine in model systems to address these questions.

The current work monitors tryptophan fluorescence as a function of pH and salt concentration to quantify the nonspecific binding of cationic peptides to single-stranded RNA in response to protonation changes of histidine and the α-amino group. Because histidine and the α-amino group are the only two basic amino acid residues which titrate near physiological pH, they are also the most likely to show any potential linkage effects between protonation and nucleic acid binding sometimes observed in native protein−nucleic acid binding processes (*25*−*29*). We examine whether protonation of histidine and the α-amino group is coupled to or independent of nonspecific RNA binding and discuss coupled protonation events within the protein−nucleic acid binding interface in the context of recent hydration studies.

BACKGROUND

McGhee−von Hippel Analysis of the Oligopeptide−DNA Binding Isotherm. The nonspecific, primarily Coulombic interactions between polyanionic nucleic acids and a variety of oligocations and proteins, including polyamines and oligopeptides similar to those studied here (*4*−*6*, *8*, *30*−*36*) are well described by the noncooperative McGhee−von Hippel (*30*) binding isotherm,

$$K_{obs} = \frac{\nu}{L_F(1-n\nu)}\left(\frac{1-(n-1)\nu}{1-n\nu}\right)^{n-1} \quad (1)$$

This form of the McGhee−von Hippel equation assumes noncooperative site binding of a linear ligand of arbitrary length to a linear, homogeneous infinite lattice with overlapping potential binding sites. In this case, the lattice is polyU and the ligand is the XWKK oligopeptide. L_F is the free ligand concentration.

The site size (n) represents the number of adjacent phosphates (i.e., lattice residues) occluded by the binding of a single oligopeptide to the RNA. The ligand binding density (ν) represents the fraction of a ligand bound per lattice residue.

The McGhee−von Hippel isotherm and its finite lattice analogue (*37*) have been extensively used to interpret fluorescence data (local accumulation of ligand) and equilibrium dialysis (global accumulation of ligand) for oligocation−nucleic acid interactions. Specific examples include fluorescence studies with oligolysines (*4*, *6*, *34*, *35*) and oligoarginines (*13*) and equilibrium dialysis studies with oligolysines (*9*, *10*), polyamines, Mg^{2+} (*32*), and $Co(NH_3)_6^{3+}$ (*31*). Monte Carlo and Poisson−Boltzmann calculations modeling the nonspecific Coulombic accumulation of a divalent cation (Mg^{2+}) in the vicinity of polynucleotides over a range of univalent salt concentration from 10−100 mM are well described by a McGhee−von Hippel isotherm with a site size between 2 and 3 (*38*). Although the McGhee−von Hippel isotherm was derived for site binding of a ligand and does not explicitly consider Coulombic or polyelectrolyte effects, its application to oligocation−polyanion data yield physically reasonable site sizes and binding constants. A comparison of the McGhee−von Hippel isotherm with alternative polyelectrolyte-based expressions for an oligocation−polyanion binding isotherm (*39*−*41*) is provided by Ni et al. (*38*).

Lohman and co-workers developed a quantitative fluorescence titration protocol that has been used extensively to obtain thermodynamic binding parameters of protein−nucleic acid interactions and is readily applied to oligopeptide−DNA/RNA binding (*4*−*6*, *13*, *34*, *42*, *43*). For ligands including *E. coli* SSB protein and various small oligopeptides, Lohman and co-workers found that the fractional fluorescence quenching (Q_{obs}/Q_{max}), where Q_{max} is defined as the maximum quenching of the oligopeptide obtained at saturation, was equal to the fraction of ligand bound (L_B/L_T),

$$\frac{Q_{obs}}{Q_{max}} = \frac{L_B}{L_T} \tag{2}$$

From eq 2, ν and L_F of the McGhee−von Hippel equation (eq 1) can be expressed in terms of experimentally accessible variables,

$$\nu \equiv \frac{L_B}{R_T} = \left(\frac{Q_{obs}}{Q_{max}}\right)\left(\frac{L_T}{R_T}\right) \tag{3}$$

$$L_F = \left(1 - \frac{Q_{obs}}{Q_{max}}\right)(L_T) \tag{4}$$

L_T and R_T are the total concentrations of ligand and RNA phosphate, and L_B is the concentration of bound ligand (*4*, *6*).

Effects of 1:1 Salt Concentration on K_{obs}. Binding interactions of nucleic acids with charged ligands are highly sensitive to salt concentration. At low to moderate salt concentrations ([NaCl] < 0.5 M), DNA and RNA binding constants of oligocations and proteins typically exhibit a power-law dependence on the activity (concentration) of univalent salt which can be expressed as the log−log derivative

$$SK_{obs} \equiv \left(\frac{\partial \log K_{obs}}{\partial \log[Na^+]}\right) \cong \Delta\Gamma_+ + \Delta\Gamma_- \tag{5}$$

where the $\Delta\Gamma$ terms are differences in preferential interaction coefficients for the interaction of the Na^+ cation ($\Delta\Gamma_+$) and the Cl^- anion ($\Delta\Gamma_-$) with the complex vs the uncomplexed reactants in the oligocation−nucleic acid binding process. SK_{obs} quantifies the thermodynamic consequences of the differences in preferential interactions of the monovalent salt ions (i.e., Na^+ and Cl^-) with the complex and with the reactants (*36*, *44*, *45*). Below 0.25 M salt, the nature of the monovalent salt ions does not significantly impact SK_{obs} for $Z_L < 10$ ligands binding to polyU (*4*, *6*), allowing comparisons of SK_{obs} across experimental systems even when obtained using different monovalent salts.

For the binding of a homologous series of cationic oligopeptides and polyamines to polyanionic DNA or RNA, $\log K_{obs}$ varies linearly as a function of $[Na^+]$

$$\log K_{obs} = \log K_0 + (SK_{obs})\log[Na^+] \tag{6}$$

where K_0 is the extrapolated value of K_{obs} at 1 M salt (*4*, *8*, *32*). Experimentally, SK_{obs} is independent of $[Na^+]$ and proportional to Z_L, the charge on the binding surface of the oligopeptide. The large magnitude of SK_{obs} and the independence of SK_{obs} vs salt concentration result primarily from the polyelectrolyte character of nucleic acids (*35*, *46*). Record et al. (*8*) predicted a thermodynamic limiting law (low [salt]) expression for SK_{obs} for oligocation−polyanion binding

$$SK_{obs} \cong -Z_L\psi \tag{7}$$

where Z_L is the valence of the oligocation ligand and ψ represents the net thermodynamic extent of salt ion accumulation per phosphate of uncomplexed DNA (*7*, *8*, *47*, *48*). Experimentally, $\psi \approx 0.88$ for double-stranded DNA (*47*) and $\psi \approx 0.74$ for single-stranded nucleic acids (*4*, *6*). Equation 7 is a special case of the general expression for SK_{obs} in eq 5. Although derived as a limiting law, eq 7 is found to describe oligocation−polyanion binding data at higher salt concentration, possibly because of compensating salt concentration dependences of preferential interaction coefficients for the ligand and macromolecule (*36*, *49*).

Cylindrical Poisson−Boltzmann theory (*50*) and counterion condensation theory (*8*, *51*) predict that at low salt (limiting law) conditions,

$$\psi = 1 - \frac{1}{2\xi} \tag{8}$$

where the reduced axial charge density, ξ, is

$$\xi = \frac{e^2}{\varepsilon kTb} \tag{9}$$

Here, e is the electronic charge, ε is the bulk dielectric constant of water, k is the Boltzmann constant, T is the absolute temperature, and b is the axial charge spacing of the polyelectrolyte. In water at 25 °C, $\xi = 7.14/b$, where b is in units of Angstroms (Å). We use eqs 6−9 as the basis for analyzing the effects of pH on K_{obs} and SK_{obs}, as described below.

The Effects of pH on $\log K_{obs}$ and SK_{obs}.

1. Titration Curve Model. The effects of pH on the interactions of pentalysine with double-stranded DNA were shown to fit a "titration" curve model (*7*), where at fixed salt concentration, the dependence of K_{obs} on pH is determined by the pH-dependence of free ligand valence (Z_L). In this model, Z_L does not increase upon binding to nucleic acids, i.e., the pK_a of the titratable groups on the oligopeptide are not affected by binding to DNA. For the simple case of independent titratable functional

groups on the oligopeptide, the dependence of Z_L on $[H^+]$ is given by

$$Z_L = Z_L^{max} - \sum_{i=1}^{g} \frac{1}{1 + k_{i,L}[H^+]} \quad (10)$$

where Z_L is the valence at a given pH, Z_L^{max} is the maximum valence at low pH ($Z_L^{max} = 4$ in the present study), $k_{i,L}$ is the equilibrium protonation constant of the ith titratable group on the oligopeptide, and g is the number of groups titrating in the pH range of interest (*6*, *7*, *47*). Assuming that the two lysines at the C-terminal end of XWKK are always protonated at the pH and salt concentrations studied here, Z_L can be expressed as

$$Z_L = Z_L^{max} - \frac{1}{1 + k_{NH_3^+}[H^+]} - \frac{1}{1 + k_X[H^+]} \quad (11)$$

where k_X is the protonation constant for the side chain of residue X (lysine or histidine) in XWKK and $k_{NH_3^+}$ is the protonation constant for the N-terminal α-amino group. The uridylate moieties in polyU are also expected to deprotonate at sufficiently high pH, which in turn will reduce the axial charge spacing b. Taking the assumption of Mascotti and Lohman (*6*), we model the pH-dependence of b as

$$\frac{b_0}{b} = 1 + \frac{1}{1 + k_U[H^+]} \quad (12)$$

where b_0 is the average charge spacing of polyU at neutral pH and k_U is the protonation constant of uridylate.

Provided that any salt concentration dependences of $k_{NH_3^+}$, k_X, and k_U are negligible and that eq 7 for SK_{obs} is valid in the range of salt concentration of interest, the dependence of $\log K_{obs}$ on pH from eqs 6−9 is

$$\log K_{obs} - \log K_0 = -\psi\left(Z_L^{max} - \frac{1}{1 + k_{NH_3^+}[H^+]} - \frac{1}{1 + k_X[H^+]}\right)\log[Na^+] \quad (13)$$

where ψ is

$$\psi = 1 - \frac{b_0}{14.28}\left(1 + \frac{1}{1 + k_U[H^+]}\right) \quad (14)$$

and K_0 is the extrapolated binding constant in the 1 M Na^+ reference state. From eqs 7 and 11,

$$SK_{obs} = -\psi\left(Z_L^{max} - \frac{1}{1 + k_{NH_3^+}[H^+]} - \frac{1}{1 + k_X[H^+]}\right) \quad (15)$$

with ψ as defined in eq 14. In this model, any protonation state of the unbound oligopeptide can bind to RNA, with K_{obs} and the magnitude of SK_{obs} increasing with increasing protonation (i.e., greater Z_L). At sufficiently low pH where all of the sites are protonated (i.e., $Z_L = Z_L^{max}$), both K_{obs} and SK_{obs} will become insensitive to pH.

2. Coupled Protonation Model. As an extreme alternative model, if protonation of the peptide were driven by complex formation so that the bound state of the peptide was the fully protonated state, then

$$SK_{obs} = -\psi(Z_L^{max}) \quad (16)$$

predicting that SK_{obs} would be to be independent of pH. However, $\log K_{obs}$ should still decrease with an increase in pH because of the increasing thermodynamic cost of protonating groups on the oligopeptide as the pH increases. This effect should give rise to a pH-dependence of K_0 and hence of K_{obs}:

$$K_0 = K_0^0 \sum_{i=1}^{g} \frac{k_{i,L}[H^+]}{1 + k_{i,L}[H^+]} \quad (17)$$

where in the pH range of our experiments (5.2−8.7), $g = 1$ or 2 for KWKK and $g = 2$ for HWKK. K_0^0 is the 1 M Na^+ extrapolated binding constant in the limiting case when all titratable sites on the ligand are protonated. As the pH increases, K_0 decreases, thus reducing K_{obs}. Although the pH dependence of K_{obs} cannot be used to distinguish between the coupled protonation model and the titration curve model within an experimentally accessible range, the pH dependence of SK_{obs} can be so used. The titration model predicts that SK_{obs} should decrease in magnitude with increasing pH. In contrast, if protonation is coupled to binding, SK_{obs} is expected to be independent of pH.

EXPERIMENTAL PROCEDURES

Buffers and Reagents. Reagents used were reagent grade, purchased from either Sigma Chemical Company (St. Louis, MO) or Fisher Scientific (Pittsburgh, PA). All solutions were prepared with 18 MΩ/cm deionized water. All buffers contained 0.2 mM Na_2EDTA and were titrated to the indicated pH with concentrated HCl. The pH 5.2 buffer was 3 mM sodium acetate, the pH 6 buffer was sodium cacodylate, pH 7−8 buffers were 3 mM sodium HEPES, and the pH 8.7 buffer was 2.5 mM sodium borate. "High salt" and "low salt" solutions were prepared with 0.2 mM Na_2EDTA and the specified buffer, with and without 1 M NaCl, respectively. Intermediate salt concentrations at a given pH were obtained using linear combinations of the low salt and high salt buffers.

Peptides. Oligopeptides of the general form XWKK, where the α-amino terminus is positively charged, the C-terminus is capped as an amide, and "X" is lysine or histidine, were synthesized, purified, lyophilized, and validated by matrix-assisted laser desorption ionization mass spectroscopy by the University of Maryland Biopolymer Core Facility. Stock peptide concentrations were determined spectrophotometrically from the 280 nm absorbance of the tryptophan in 6 M guanidinium chloride using ε_{280}^{Trp} = 5690 M^{-1} cm^{-1} (*52*). The extinction coefficients of the oligopeptides dissolved in the buffers described above (3−5 mM Na^+) were then experimentally measured for use in determining the inner-filter corrections (see above) for the fluorescence titrations performed (ε_{292}^{HWKK} = 3380 ± 50 M^{-1} cm^{-1}, ε_{292}^{KWKK} = 3140 ± 110 M^{-1} cm^{-1}, ε_{350}^{XWKK} < 5 M^{-1} cm^{-1}). The resulting inner-filter correction is small relative to the corresponding correction due to the RNA concentration (see below).

polyU Single-Stranded RNA. The potassium salt of polyuridylic acid (polyU) was manufactured (lot no. 011805) by the Midland Certified Reagent Company (Midland, TX). After synthesis, phenol/chloroform/isoamyl alcohol extraction and extensive dialysis against potassium chloride, the polyU was exhaustively dialyzed against deionized water to remove excess salt and then lyophilized by the manufacturer. Analytical polyacrylamide gel electrophoretic analysis indicated that the polyU substrates ranged between 40−200 bases in length. Studies of the transition between oligomeric vs polymeric binding for oligopeptides associating with single stranded nucleic acids found that

a ligand with $Z_L \leq 4$ binds the central site of a nucleic acid with 22 or more charges with the same affinity as the central site of a polymeric nucleic acid (*53*, *54*). As such, XWKK is predicted to bind this distribution of polyU lengths equivalently in the low binding density limit reported by the McGhee−von Hippel isotherm (*23*). Extinction coefficients of the RNA were determined for use with the inner-filter corrections ($\varepsilon_{292}^{RNA} = 160 \pm 40$ M^{-1} cm^{-1}, $\varepsilon_{350}^{RNA} \sim 0$ M^{-1} cm^{-1}). The inner-filter correction (*42*) due to the RNA concentration in the cuvette can result in as much as a 17% change in fluorescence intensity.

Bioinformatics. Sequence alignments were prepared using the CLUSTALW version 3.2 software package available via the Internet at the San Diego Supercomputing Center Workbench (http://www.workbench.sdsc.edu).

Fluorescence Quenching Studies of Oligopeptide Binding. Oligopeptide binding to polyU was monitored by tryptophan fluorescence quenching with a Cary Eclipse spectrofluorometer (Varian Instruments) equipped with a Peltier temperature controller maintaining solution at 25 °C. The excitation wavelength was 292 nm with a bandpass of 2.5 nm, and the emission wavelength was 350 nm with a bandpass of 10 nm. These wavelengths were chosen to minimize the inner-filter corrections and RNA absorbance (*42*). Solutions of the oligopeptides and RNA used in the fluorescent titrations were prepared from freezer stocks and diluted to identical buffer and salt concentration conditions. All titrations were performed in 1 cm × 1 cm square quartz cuvettes to allow for "crown" stir-bar mixing during titration and measurement. After addition of titrant (either with polyU during the "reverse titration" or with "high salt" buffer during "saltbacks") to the oligopeptide solution, samples were incubated with stirring for at least one minute before measurement. Photobleaching of tryptophan in XWKK was minimized by illuminating the sample only during measurement. For comparison, unbound KWKK and HWKK exhibited less than 3% loss in fluorescence after an hour of continuous irradiation (data not shown). To correct for Raman light scattering from the water and any background fluorescent emission, the fluorescence of a buffer solution (no oligopeptide present) that was at the equivalent RNA and salt concentration in the titration was subtracted from the fluorescent signal of the sample. The extent of tryptophan fluorescence quenching is thus defined as

$$Q_{obs} \equiv \frac{F_0 - F_{obs}}{F_0} \quad (18)$$

where F_{obs} is the observed fluorescence intensity at a given point in the titration and F_0 is the initial fluorescence intensity of the free ligand (i.e., oligopeptide). All fluorescence intensities were corrected for background fluorescence, dilution, inner-filter contributions, and photobleaching effects as described previously (*35*, *42*).

Reverse Titrations. Isotherms of either HWKK or KWKK binding to polyU were generated by "reverse titration", where 1−10 mM stock solutions of RNA were titrated into cuvettes containing 1−8 μM of XWKK. Titrations continued until binding saturation was observed or a maximum concentration of 0.3 mM RNA phosphate was achieved, a limit dictated by the approximations used for inner-filter correction. Values of Q_{obs} (eq 18) as a function of XWKK and polyU concentrations were then used to calculate binding affinity (see below).

HWKK deprotonates to a greater extent relative to KWKK within the range of pH considered, resulting in decreased binding affinity at moderate and high pH values. To maintain oligopeptide−RNA binding affinity within measurable limits yet allow for direct comparison of binding affinities across the full pH range, titrations were performed at the common salt concentrations of 24.4 mM Na^+ for KWKK and 9.8 mM Na^+ for HWKK (Table 1).

Table 1: pH Dependence of McGhee−von Hippel $\log K_{obs}$ and SK_{obs} as a Function of Amino Acid Composition

pH	$\log K_{obs}$ [a]	SK_{obs} [b]	$\log K_0$ [b] (1 M Na^+)	Q_{max} [c] (%)
		KWKK (24.4 mM Na^+)		
5.2	5.06 ± 0.02	−3.06 ± 0.09	0.10 ± 0.12	0.91 ± 0.01
6.0	4.88 ± 0.01	−3.05 ± 0.06	0.01 ± 0.09	0.91 ± 0.01
7.0	4.69 ± 0.02	−2.94 ± 0.06	−0.06 ± 0.08	0.91 ± 0.02
8.0	4.16 ± 0.01	−2.59 ± 0.06	−0.01 ± 0.09	0.91 ± 0.02
8.7	3.77 ± 0.02	−2.45 ± 0.11	−0.13 ± 0.17	0.87 ± 0.01[d]
		HWKK (9.8 mM Na^+)		
5.2	5.98 ± 0.02	−2.84 ± 0.10	0.25 ± 0.15	0.92 ± 0.02
6.0	5.23 ± 0.02	−2.55 ± 0.09	0.09 ± 0.12	0.93 ± 0.01
7.0	4.59 ± 0.02	−2.21 ± 0.06	0.11 ± 0.11	0.93 ± 0.01
8.0	3.83 ± 0.02	−1.93 ± 0.07	−0.01 ± 0.12	0.88 ± 0.01[e]
8.7	3.38 ± 0.02	−1.64 ± 0.13	0.14 ± 0.24	0.81 ± 0.02[e]

[a]Determined by global nonlinear least-squares analysis of data collected at 25 °C across multiple oligopeptide concentrations at the specified salt concentration using the noncooperative McGhee−von Hippel equation (eq 1) with the indicated Q_{max} and $n = 5$. Errors represent 95% confidence intervals. [b]SK_{obs} and log K_0 values were calculated by nonlinear least-squares analysis of aggregate $\log K_{obs}$ vs [Na^+] data from reverse titrations and saltbacks. Saltback $\log K_{obs}$ data were obtained using the indicated Q_{max} and $n = 5$ via eqs 1−4. [c]Calculated via model-independent ligand binding density analysis (*42*) of reverse titration data at the specified salt concentration. [d]When binding was weaker than $K_{obs} \lesssim 10^4$ M^{-1}, Q_{max} was found by ligand binding density analysis using data collected at the same pH but lower salt concentration to improve the accuracy of the determination (cf. Figure S1, Supporting Information). At high pH, Q_{max} is reported at 12.4 mM Na^+ (denoted by [d]) for KWKK. [e]When binding was weaker than $K_{obs} \lesssim 10^4$ M^{-1}, Q_{max} was found by ligand binding density analysis using data collected at the same pH but lower salt concentration to improve the accuracy of the determination (cf. Figure S1, Supporting Information). At high pH, Q_{max} is reported 5.4 mM Na^+ (denoted by [e]) for HWKK.

Saltback Titrations. Salt concentration dependences of the oligopeptide−RNA binding equilibrium were determined in part via "saltback" titrations where the pre-equilibrated XWKK−RNA complex was titrated with the "high salt" buffer with the appropriate pH (see Buffers and Reagents section above), monitoring the increase in fluorescence and therefore the decrease in quenching Q_{obs} as the salt concentration of the solution increases. After all corrections were applied (i.e., background fluorescence, dilution, inner-filter, photobleaching), more than 90% of the original fluorescence of the free oligopeptide is recovered, indicative of the reversibility of oligopeptide−RNA complex formation. SK_{obs} and $\log K_0$ values determined by saltback titrations were supported by at least three independent reverse titration determinations of K_{obs} at various salt concentrations, with each K_{obs} derived from at least three isotherms (see below and Figure 5).

Analysis of Oligopeptide−RNA Binding Isotherms. The binding constant K_{obs} was determined from reverse titration data by fitting to the noncooperative McGhee−von Hippel (*30*) binding isotherm (eq 1). The parameters ν and L_F were determined via eqs 2−4. Q_{max} was calculated by global analysis of 3−7 isotherms for XWKK concentrations ranging between 1−8 μM using the model-independent method of ligand binding density (LBD) analysis (*42*). The nonlinear

Table 2: Global Fit Parameters Describing the pH Dependence of $\log K_{obs}$ and SK_{obs} vs Amino Acid Composition[a]

			pK_a	
peptide	ψ	$\log K_0$ (1 M Na^+)	histidine	αNH_3^+
KWKK	0.77 ± 0.01	0.02 ± 0.07		7.57 ± 0.08
HWKK	0.76 ± 0.03	0.12 ± 0.10	5.75 ± 0.18	7.86 ± 0.13

[a]Parameters reported are the globally fitted values to eq 13 for all reverse titration and saltback data in Figure 5 ($N \approx 70-71$ data points each). Errors represent 95% confidence intervals for the global fit.

least-squares program NONLIN (*55*) was used to fit $\log K_{obs}$ and n to eqs 1−5 using a fixed Q_{max} obtained by LBD analysis. Q_{max} converged to the LBD-determined value when allowed to float for titrations where $K_{obs} \gtrsim 10^5\ M^{-1}$ and in global analysis of multiple reverse titrations across 4−6 salt concentrations (data not shown). The site size parameter, n, was typically not integral when allowed to float during nonlinear fitting. Any Coulombic or other source of negative or positive cooperativity that may exist has effectively been absorbed by n and these factors may be responsible for the nonintegral n. Nevertheless, no dependence of n on the values of ν or L_F has been found in this or previous studies. Site size was indistinguishable from or near $n = 5$ in global analysis of reverse titration data obtained at a common pH (Table SI, Supporting Information). The $n \approx 5$ site size was also determined using a model-independent approach (see Results). Unless otherwise indicated, binding constants and their salt dependence are reported using a site size fixed at $n = 5$.

$\log K_{obs}$ as a function of salt concentration was directly calculated for saltback data via eq 1 using a constant Q_{obs} determined by LBD analysis and site size $n = 5$. To facilitate comparison of HWKK vs KWKK binding to polyU in Figure 6, $\log K_{obs}$ data for HWKK at 24.4 mM Na^+ was linearly interpolated via eq 6 and the SK_{obs} and $\log K_0$ parameters listed in Table 1. All K_{obs} data (Figure 5) were globally fit to eq 13 as a function of salt concentration and pH, with parameters listed in Table 2.

Statistical Comparison of Fitting Parameters and Thermodynamic Models. Several times in this study, we assess whether adding complexity to our models dramatically improves the description of the data. The *F*-test is a common means to determine the statistical significance of adding terms to nested models (i.e., a series of models where fixing parameters to some value such as 0 or 1 generates a simpler expression from a more complex one). However, both the McGhee−von Hippel isotherm (eq 1) and the titration binding model (eqs 13−15) are nonlinear equations where terms cannot be eliminated by setting a parameter to a constant value. The second-order Akaike information criterion (AIC_c) (*56*, *57*) is a well accepted alternative to the *F*-test, which does not have the nested-model restriction:

$$AIC_c = N \ln\left(\frac{SS_{res}}{N}\right) + 2(p+1) + \frac{2(p+1)(p+2)}{N-p-2} \qquad (19)$$

In eq 19, N is the number of data points, SS_{res} is the residual sum of squares of the fit, and p is the number of parameters in the model. The AIC_c is calculated for each model considered. For two models "A" vs "B", the better model has a smaller (or more negative) AIC_c. When AIC_c scores are close in value, the probability that one model is favored over the other is defined by

$$\text{probability} = \frac{e^{-\Delta AIC_c}}{1 + e^{-\Delta AIC_c}} \qquad (20)$$

where $\Delta AIC_c = AIC_{c,B} - AIC_{c,A}$. The evidence ratio (also called the relative likelihood) is the ratio of the probability (eq 20) favoring model "A" vs the probability favoring "B." The evidence ratio can be calculated directly by $e^{0.5\Delta AIC_c}$ because the ΔAIC_c values for these two cases are related by a sign inversion. As an example, if "A" is favored over "B" with a $\Delta AIC_c = 6.0$, model "A" has a ~95% probability of being a better description of the data in comparison to "B" (with a ~5% chance). The evidence ratio of A/B states that "A" is 20-fold more likely than "B" to be the correct model (*56*). Model comparisons are reported using ΔAIC_c or evidence ratios if ΔAIC is small. We arbitrarily define that a model is convincingly preferred when ΔAIC_c has a magnitude of 6.0 or greater (evidence ratio ≥20).

RESULTS

The work presented here compares polyU binding by HWKK, which has not been studied before, with the previously characterized KWKK (*4*−*6*, *13*) to determine how the change from lysine to histidine affects binding affinity K_{obs} (eq 1), its salt dependence SK_{obs}, and site size over a range of pH in which histidine and the α-amino group deprotonate. Titrations under stoichiometric binding conditions were used to determine a model-independent site size of XWKK on polyU (Figure 2). The titrations were performed at low salt (3.4 mM Na^+) and low pH (pH 5.2) to maximize binding affinity ($\log K_{obs} \geq 7.3$). The site size is indicated by the intersection of the polyU concentration-dependent regime with the polyU concentration-independent plateau. The invariance of the intersection point across three titrations over a 2-fold concentration range suggests that $n \approx 5$ is a true site size for KWKK and HWKK binding to polyU at pH 5.2.

Figure 3 shows a typical series of reverse titration binding isotherms. As the initial oligopeptide concentration is increased, increasing amounts of polyU are required to achieve an equivalent level of binding saturation. The HWKK isotherms are well described by the noncooperative McGhee−von Hippel model, as has been shown for KWKK (*4*−*6*, *13*), Mg^{2+} (*8*) and model peptides (*34*, *46*) bind to nucleic acids with McGhee−von Hippel site sizes approximately equal to the net charge of the ligand. However, constraining the site size to $n = 4$, the number of ligand charges neutralized in the XWKK−polyU complex, results in a statistically poorer fit relative to $n = 5$ (Figure 3, dashed vs solid lines; Table S1, Supporting Information). Site size converges to $n \approx 5$ when allowed to float as a parameter (Table S1, Supporting Information; Figure 3, solid lines), consistent with the model-independent determination of site size in Figure 2. At pH 6, increasing n from 4 to 5 increases K_{obs} 35% and decrease ΔG^o by about 3%; this site size effect on K_{obs} continues to decrease at higher pH.

Calculation of binding affinity requires knowledge of how binding density ν varies as a function of free oligopeptide concentration L_F. Q_{obs} can be directly related to ν and L_F through Q_{max} (eqs 3−4). The upper asymptote, and thus Q_{max}, is easily defined when binding is saturable (e.g., at low pH and/or low [Na^+]; cf. HWKK at pH 5.2 in Figure 4). However, with weaker binding, uncertainty in the estimation of Q_{max} from a single isotherm dramatically increases as the upper asymptote becomes more difficult to reach. Ligand binding density (LBD)

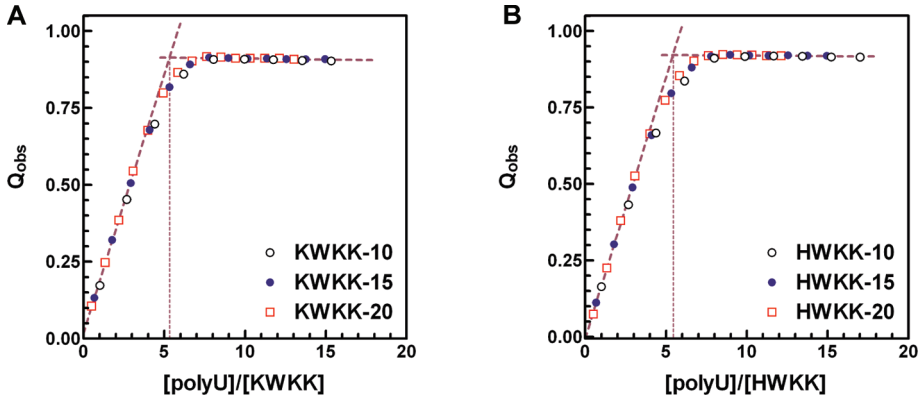

FIGURE 2: Determination of XWKK site size on polyU by stoichiometric binding. Titrations of (A) KWKK or (B) HWKK as a function of initial oligopeptide concentration (see respective legends above) at 3.4 mM Na^+ and 25 °C (i.e., high affinity conditions). Intersection of the linear least-squares fits of the two regimes (dashed purple lines) is indicated by a light-purple dotted line for clarity. The intersections indicate a site size $n = 5.3 \pm 0.1$ for KWKK and $n = 5.4 \pm 0.1$ for HWKK.

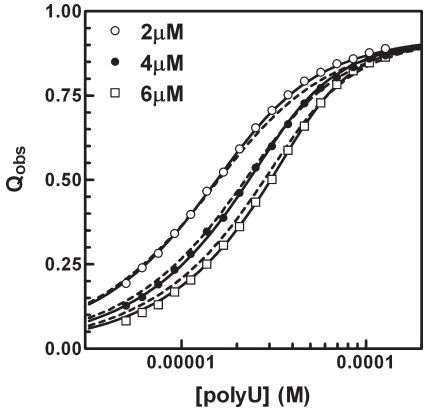

FIGURE 3: Titrations of the oligopeptide HWKK with polyU. Titrations at three HWKK concentrations (2 μM (○), 4 μM (●), and 6 μM (□)) observed as function of tryptophan fluorescence quenching (eq 14) at 9.8 mM Na^+, pH 6.0, and 25 °C. The concentration of polyU is given in moles of nucleotides per liter. Solid and dashed lines are the nonlinear least-squares global fits across all three titrations using eqs 1, 3, and 4, with $Q_{max} = 0.93$ as determined by ligand binding density analysis (*35*). The dashed line reports the McGhee−von Hippel isotherm with $\log K_{obs} = 5.11 \pm 0.02$ with a site size fixed at $n = 4$. The solid line isotherm shows the fit with the site size allowed to float ($\log K_{obs} = 5.22 \pm 0.02$, $n = 4.96 \pm 0.11$). If all parameters are allowed to float, $\log K_{obs} = 5.23 \pm 0.03$, $Q_{max} = 0.929 \pm 0.007$, and $n = 4.97 \pm 0.13$ (data not shown in plot above).

analysis provides a model-independent means of determining Q_{max} and other thermodynamic parameters (*42*, *58*). Mascotti and Lohman applied LBD analysis to nucleic acid binding studies of a series of oligopeptides KWK_x ($x = 1-8$), including KWKK. Figure S1 of the Supporting Information presents the results of LBD analysis of KWKK and HWKK, plotting Q_{obs} as a function of L_B/L_T. Because Q_{obs} is a linear function of the fraction of peptide bound (L_B/L_T), eq 3 shows that binding density ν is also a linear function of Q_{obs}, and by extension, L_F can be calculated using eq 4. Extrapolation of L_B/L_T to 1 allows calculation of Q_{max} without requiring XWKK binding saturation. Q_{max} was insensitive to salt concentration in the range considered (data not shown). Q_{max} was relatively constant over pH 5.2−7, decreasing at pH 8 for HWKK and pH 8.7 for KWKK (Table 1 and Figure S1 of the Supporting Information). The pH dependence of XWKK Q_{max} is consistent with previous reports showing that Q_{max} was proportional to net oligopeptide charge for a series of oligolysines ($Z_L \leq 4$) binding to polyU (*6*), suggesting that tryptophan fluorescence quenching is modulated by net differences in adjacent charge, whether by deprotonation in the case of XWKK, or by the presence of additional lysines at the C-terminus as seen in the work of Mascotti and Lohman (*6*).

Using Q_{max} determined by LBD analysis and eqs 2−4 to calculate ν and L_F, we assessed the pH sensitivity of XWKK−polyU binding for HWKK relative to KWKK (Figure 4). KWKK binding is only moderately affected at low pH, with marked decreases at pH 8 and 8.7. In contrast, $\log K_{obs}$ for HWKK is a strong function of pH and is weaker than KWKK at neutral pH even at a relatively lower salt concentration which favors tighter binding (9.8 mM Na^+ vs 24.4 mM Na^+). With the exception of HWKK at pH 7.0, which has a fitted $n = 4.36 \pm 0.36$, the McGhee−von Hippel site size is invariant at $n = 5.0$ within error across the full 5.2−8.7 pH range for both HWKK and KWKK (Table S1, Supporting Information).

The linear dependence of Q_{obs} on binding density and the apparent invariance of site size across salt concentration and pH permits simple calculation of K_{obs} from eqs 1, 3, and 4 for a given Q_{obs}. In cases where NaCl titration of preformed XWKK−polyU complexes results in full recovery of the initial tryptophan fluorescence, "saltback" titrations provide a much more direct route to calculating the salt dependence of $\log K_{obs}$ via eq 6. Figure 5 presents the $\log K_{obs}$ data as a function of salt concentration and pH for KWKK and HWKK. Black symbols represent reverse titration data measured and analyzed across 3−7 oligopeptide concentrations, while red symbols indicate log K_{obs} values determined via the saltback methodology (*42*). The colinearity of $\log K_{obs}$ vs $\log[Na^+]$ data observed by reverse titration vs saltback approaches suggests that saltback measurements accurately reflect the salt dependence of polyU-binding affinity for KWKK and HWKK. In light of this observation, the reverse titration and saltback data were analyzed as a whole. Black lines in Figure 5 represent linear least-squares fits of log K_{obs} vs $\log[Na^+]$ for each peptide and pH. Green lines indicate the predicted salt dependence of binding affinity using eq 13 and parameters determined by global nonlinear least-squares analysis of the combined $\log K_{obs}$ data from reverse titrations and saltbacks across the full pH range (Figure 5). The SK_{obs} of HWKK−polyU shows a steep magnitude decrease as pH increases (Table 1), reflected in more shallow slopes in the salt dependence of $\log K_{obs}$ in Figure 5B. KWKK in Figure 5A also

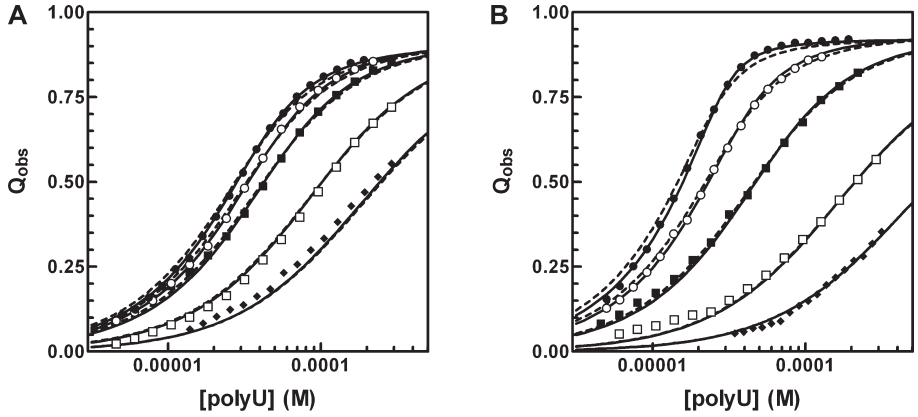

FIGURE 4: XWKK binding isotherms as a function of pH. Titrations of (A) KWKK at 24.4 mM Na^+ or (B) HWKK at 9.8 mM Na^+ as a function of polyU. Data from titrations peformed at 25 °C with 4 μM oligopeptide are presented for each pH with the following symbols: (●), pH 5.2; (○), pH 6.0; (■), pH 7.0; (□), pH 8.0; (◆), pH 8.7. Curves represent fits determined by global nonlinear least-squares analysis across all oligopeptide concentrations (2−6 μM) at the specified pH and salt concentration (cf. Figure 3). Lines represent the best global fits to the data when the site size is constrained to $n = 4$ (dashed lines) or $n = 5$ (solid lines; Table 1).

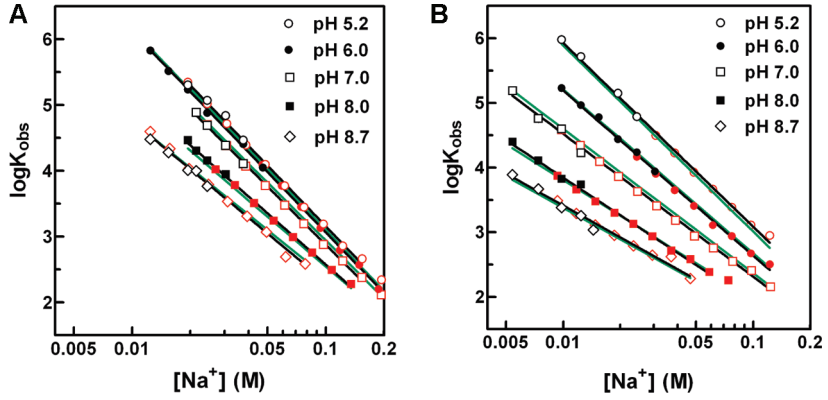

FIGURE 5: Dependence of log K_{obs} on [Na^+] and pH. log K_{obs}, determined directly by global analysis of multiple reverse titrations (black symbols) or via calculation using eqs 1, 2, and 4 and saltback data (red symbols) are plotted as a function of pH and salt concentration. Black solid lines represent linear least-squares fits of combined reverse titration and saltback data (reported in Table 1). Green solid lines indicate the predicted dependence of log K_{obs} on [Na^+] and pH using eqs 13−14 and parameters found by global nonlinear least-squares analysis of all log K_{obs} vs [Na^+] data (Table 2).

exhibits a decreased SK_{obs} magnitude at high pH, although to a lesser extent than HWKK. The small magnitude of logK_0 (the residual binding affinity at 1 M Na^+ where polyelectrolyte contributions are considered to be negligible) indicates that the polyelectrolyte effect accounts for the majority of the ΔG^o of the binding interaction for XWKK (Table 1). This is consistent with previous oligocation−nucleic acid binding studies (*4*−*8*, *11*, *32*, *35*, *46*, *53*).

XWKK binding affinity K_{obs} and its salt dependence SK_{obs} are presented in Figure 6. To facilitate comparison to the KWKK logK_{obs} data, HWKK logK_{obs} values were interpolated to 24.4 mM Na^+ by eq 6 using the SK_{obs} and logK_0 parameters reported in Table 1. The same global analysis, which generated the green logK_{obs} vs log[Na^+] fits in Figure 5, are presented as a function of pH in Figure 6. At low pH, K_{obs} of HWKK approaches K_{obs} of KWKK, indicating that the nucleic acid binding free energy contribution of protonated histidine is similar to that of lysine. The titration model (eqs 13−15) is overwhelmingly favored over the proton-uptake model (eqs 16−17) to describe the pH dependence of polyU-binding for KWKK (evidence ratio = 2×10^{19}) and HWKK (evidence ratio = 2×10^{39}). In other words, the titration model, which couples changes in the oligopeptide charge Z_L (eq 10) to SK_{obs} through ψ (eq 7) and thus to logK_{obs} by eq 6, describes all of the observed binding phenomena for both HWKK and KWKK across changes in salt concentration and pH. The net thermodynamic ion accumulation around each polyU phosphate was equivalent for KWKK and HWKK with $\psi^{KWKK} = 0.77 \pm 0.01$ and $\psi^{HWKK} = 0.76 \pm 0.03$ (Table 2), consistent with literature values for KWKK ($\psi = 0.78 \pm 0.05$) and its KWK_x variants (composite $\psi = 0.74 \pm 0.04$) at pH 6 (*4*, *6*).

With increasing pH, HWKK−polyU binding exhibits two observable deprotonation events with pK_a values of 5.75 ± 0.18 and 7.86 ± 0.13 for the histidine imidazole and the α-amino group, respectively. The fitted α-amino pK_a for KWKK was 7.57 ± 0.08, in agreement with previous results (*6*). Accounting for potential lysine ε-NH_3^+ deprotonation at pH > 8 by adding a second titration term to the fixed-ψ model provides a minor improvement to the fit as judged by comparison of the second-order Akaike information criteria (AIC_c) with a only 78% probability favoring the two pK_a fixed-ψ model (evidence ratio = 3.5). Additional model complexity compensating for uracil deprotonation through eq 14 was not necessary for HWKK (99% probability favoring the fixed-ψ model; evidence ratio = 79.1) or the two-pK_a model for KWKK (37% favoring the 2-pK_a titrating-ψ model with $\Delta AIC_c = 1.05$; evidence ratio = 1.7).

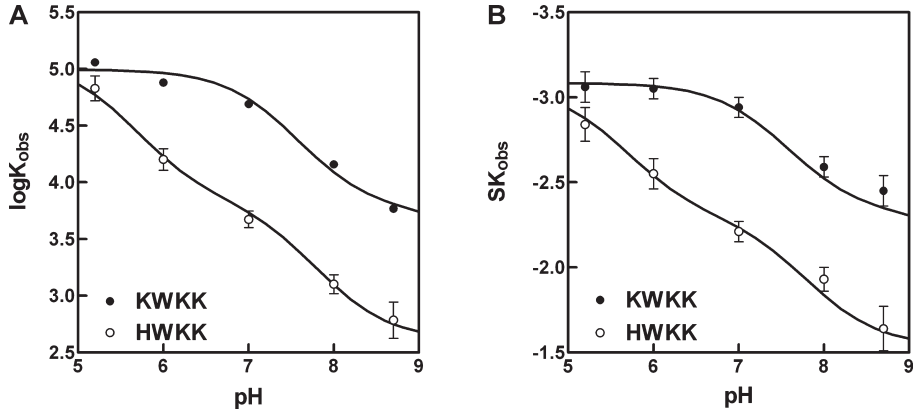

FIGURE 6: Model description of XWKK−polyU logK_{obs} and SK_{obs} vs pH. (A) logK_{obs} for XWKK binding to polyU at 25 °C and 24.4 mM Na^+ are plotted as a function of pH. KWKK logK_{obs} was directly determined from reverse titration data (●), whereas HWKK logK_{obs} (○) was interpolated via eq 6 using the parameters in Table 1. Curves represent the global nonlinear least-squares fit of the combined logK_{obs} vs [salt] and pH data in Figure 6 to eq 9 (Table 2). (B) SK_{obs}, as reported in Table 1, is plotted as a function of pH for KWKK and HWKK. Curves represent the fits to eq 13−14 using the parameters in Table 2.

However, fitting KWKK to the single-pK_a model was dramatically improved by using eq 14 in lieu of a fixed-ψ model ($\Delta AIC_c = 38.4$). Including the potential deprotonation of uracil (eq 14) or of lysine by increasing $g = 1$ to $g = 2$ in eq 10 contributes another KWKK−polyU titration event with a p$K_a \geq 9.6$ (Figure S2, Supporting Information). Inspection of Figure S2 (Supporting Information) suggests that the KWKK preference for an additional alkaline pK_a is dictated predominantly by the pH 8.7 data. Indeed, all other KWKK−polyU fitted parameters (α-amino pK_a, log K_0, and ψ fitted directly or through eq 14 via b_0) were equivalent within error across the four model variants. Taking all of these factors in consideration, we chose the fixed-ψ mode using a single titratable group for KWKK and two titratable groups for HWKK to describe XWKK binding data in Figures 5−6 and Table 1.

DISCUSSION

Protonation of Histidine and N-Terminal α-Amino Residues on HWKK and KWKK Is Not Required for Binding to polyU. This study determines whether nonspecific nucleic acid-binding exhibits pK_a shifts of titratable amino acid moieties in histidine- and lysine-containing peptides. Three observations indicate that both KWKK and HWKK bind to polyU without pK_a shifts and coupled uptake of protons. First and foremost, the pK_a values found here for histidine, lysine, and the α-amino group are consistent with pK_a measurements for free oligopeptides. Second, the magnitude of SK_{obs} decreases with increasing pH (Figures 5−6), indicating that the number of positive charges and therefore the protonation state of HWKK and KWKK in the complex with polyU decreases with increasing pH, consistent with the titration model (eq 15) and not the coupled protonation model (eq 16). Finally, log K_0, which is small in magnitude and does not vary significantly with increasing pH, does not reflect the decrease in K_0 predicted by the coupled protonation model (eq 17) to account for the enthalpic cost of stabilizing the peptide−polyU complex by proton uptake. Our demonstration that histidine and α-amino group protonation is intrinsically uncoupled from nonspecific nucleic acid binding indicates that the histidine pK_a shifts observed for many specific protein−nucleic acid recognition processes require additional noncovalent interactions to stabilize the protonated state which are not available in generalized nonspecific binding interfaces.

Histidine−polyU Binding Thermodynamics are Well Described by Limiting Law Polyelectrolyte Theory. Polyelectrolyte theory developed in the limit of low monovalent salt concentration and near-zero macromolecule binding density accurately describes XWKK−polyU binding between pH 5.2−8.7 and 5.4−200 mM Na^+. The nonelectrostatic binding constant K_0 at 1 M Na^+ was indistinguishable from zero for both HWKK and KWKK as expected for a Coulombic interaction entropically driven by salt ion release, consistent with previous model studies (*4*−*6*, *32*, *36*, *44*). The contributions of protonated histidine and protonated lysine to binding free energy are the same within uncertainty. From the perspective of the nucleic acid, the polyU per-phosphate ion accumulation is equivalent within error for $Z_L = 4$ oligopeptides HWKK ($\psi = 0.76 \pm 0.03$), KWKK ($\psi = 0.77 \pm 0.01$), and the arginine-containing oligopeptide RWRR ($\psi = 0.80 \pm 0.05$) (*13*). If ψ is expressed as a function of the polyU axial charge spacing through eq 14, values of $b_0 = 3.2 \pm 0.2$ Å and 3.3 ± 0.3 Å obtained from the salt dependence of binding for KWKK and HWKK respectively (Figure S2, Supporting Information) are consistent with a previous report of $b_0 = 3.2 \pm 0.6$ Å for single-stranded polyU and poly(rA) obtained by analysis of nucleic acid folding-unfolding processes (*59*). The reproducibility of ψ and b_0 determined for differing processes (binding vs melting) and with ligands with varying amino acid composition (lysine, arginine, or histidine) indicate that ψ and b_0 are thermodynamic parameters entirely dictated by the polyelectrolyte character of polyU. With $\log K_0 \approx 0$ and $\psi \approx 0.78$, HWKK−polyU binding and its dependence on salt concentration and pH are fully explained by changes in the protonation state of histidine and the N-terminal α-amino group.

Protonation States of Amino Acid Moieties Are Tunable. Statistically validated differences in the α-amino pK_a for HWKK vs KWKK indicate that replacing the neighboring lysine moiety with histidine promotes a pK_a shift (Table 2). Fitting HWKK data with a pK_a held constant using the p$K_a = 7.57$ from KWKK is strongly disfavored ($\Delta AIC_c = 8.6$; evidence ratio = 75.4), while the converse constraint of fitting KWKK data with the HWKK p$K_a = 7.81$ results in an even poorer fit ($\Delta AIC_c = 20.0$; evidence ratio = 1.3×10^5). The decreased acidity of the α-amino group in HWKK relative to KWKK likely reflects the reduced free energy cost of adjacent charge−charge repulsion due to prior histidine deprotonation.

Analogous to our findings that the α-amino group pK_a depends on adjacent sequence in XWKK, numerous reports show that histidine protonation equilibria are sensitive to local environment changes (*28*, *60*−*63*). The highly tunable nature of histidine protonation in native proteins is exemplified by sperm whale myoglobin which possesses seven histidines with pK_a values ranging between 5.13−8.08 (*60*). Histidine pK_a variations for a series of model peptides based on sequences from sperm whale myoglobin were assessed at 0.02 M NaCl and 25 °C by NMR spectroscopy (*60*). Flanking lysines in Phe-Lys-His-Leu-Lys (FKHLK) acidify the adjacent histidine by $\Delta pK_a = -0.52$ relative to Gly-His-Gly (GHG) ($^{His}pK_a = 6.16 \pm 0.02$ vs 6.68 ± 0.02, respectively). Proline isomerization from *cis* to *trans* in Lys-Ser-His-Pro-Glu (KSHPE) suppresses histidine deprotonation with a $\Delta pK_a = +0.46$ from 6.23 ± 0.02 to 6.69 ± 0.02, likely due to the difference in relative orientation of glutamate and histidine residues. These findings demonstrate that simple electrostatic differences in the vicinity of histidine are sufficient to modulate its protonation pH dependence in either direction. However, the histidines in FKHLK and KSHPE exhibit further pK_a perturbations in the context of native protein structure. FKHLK and KSHPE are the respective oligopeptide models for His36 and His48 in sperm whale myoglobin (*60*). His36, only observed in the *trans* conformation in the wild-type protein, has a $pK_a = 7.67 \pm 0.02$, which is $\Delta pK_a = +0.98$ more basic than its corresponding model peptide, *trans*-KSHPE. Similarly, His48 is more acidic in sperm whale myoglobin ($pK_a = 5.42 \pm 0.02$), reflecting a $\Delta pK_a = -0.74$ relative to FKHLK. The potential to tune the histidine protonation equilibrium constant across 3 orders of magnitude suggests that the prevalence of histidine at nucleic acid-binding interfaces may serve as an exquisite means to regulate protein−nucleic acid processes by providing important non-covalent interactions through coupled protonation.

Many nucleic acid-binding proteins exhibit histidine protonation coupled to binding. The pK_a of highly conserved His318 in the DNA-binding interface of human papillomavirus type 16 E2 protein (E2C) increases upon DNA binding (from 6.7 to 7.8; $\Delta pK_a = +1.1$) in a mechanism proposed to be critical for the transition from nonspecific to specific DNA recognition (*28*). The pK_a of His451 in rat glucocorticoid receptor increases from 5.9 to 7.9 after binding the phosphodiester backbone of its DNA recognition element (*25*). His203 of the origin-binding domain of SV40 T antigen (T-ag-obd) exhibits a pK_a shift from ∼5 to >8 when it binds specifically to the middle phosphate of the GAGGC pentanucleotide (*27*). His49 of the thermophile *Pyrococcus woesei* TATA-binding protein (*Pw*TBP) has a pK_a of 6.2 in the unbound state but increases to $pK_a = 7.2$ when *Pw*TBP complexes with its recognition sequence in which His49 interacts directly with a DNA phosphate (*29*). In each of the structural studies described above, proton uptake is coupled to specific binding to generate salt bridges or other interactions between the protonated histidine and complementary surfaces within the binding interface (*25*, *27*−*29*). In cases where nonspecific binding by these proteins was considered, histidine did not show these interactions (*18*, *27*, *28*). For example, His451 which exhibits a $\Delta pK_a = +2$ in the specific complex did not interact with a noncognate element (*18*). The coupled protonation of His203 with specific binding of T-ag-obd to its recognition sequence was not observed for the binding a noncognate sequence (*27*). In E2C, His322 and His326 reside in a flexible and fully solvent-exposed loop domain known to participate in long-range nonspecific electrostatic interactions with cognate DNA (*64*). However, the His322 and His326 pK_a values (6.3 and 6.2, respectively) do not change upon specific binding, whereas the nearby His318 protonates during the same process to make a hypothesized water-mediated contact to a DNA phosphate (*28*). Together, the unbound proteins highlighted above (*25*, *27*−*29*) have comparable histidine pK_a values (average $pK_a = 6.0 \pm 0.7$) to those seen for nonspecific binding histidines in E2C (*28*) and to the $pK_a = 5.75 \pm 0.18$ for HWKK nonspecific binding to single-stranded RNA seen here. We note that all of these pK_a values are nearly indistinguishable from that of free histidine ($pK_a = 6.04$ (*65*)). In addition to the proteins above which show coupled protonation upon specific binding, lac repressor (lacR) exhibits cooperative uptake of 2 protons during nonspecific binding between pH 7.7−8.4 (*26*), even though specific binding of lacR with lac operator DNA is well-described by the titration model for a single titratable group with no evidence of coupled protonation between pH 7.1−8.4 (*66*). deHaseth et al. did not identify which residues were protonated during nonspecific binding, but Kalidomos et al. observed that lacR His29 makes electrostatic contacts with a DNA phosphate in both specific and nonspecific complexes (*67*).

The striking pK_a shifts described above are likely independent of large changes in protein structure. For example, E2C does not significantly change its conformation upon specific binding of its recognition element (*68*). Several structural comparisons of protein−DNA complexes report that the distribution of protein residues interacting with DNA are overall quite similar for a given protein in specific vs nonspecific complexes, although the DNA targets of these interactions typically change (*18*, *67*, *69*−*72*). For ∼80% of the 44 specific DNA-binding proteins considered in rigid-body docking simulations, the sites involved in specific DNA recognition were also predicted to be favorable interaction sites for nonspecific DNA-binding (*72*). These combined findings suggest that protonation events coupled to specific binding are principally due to many small changes in the local environment rather than large domain rearrangements within the protein.

Structural and thermodynamic studies provide evidence that the interfaces in specifically bound protein−DNA complexes are highly dehydrated, with specific interactions between protein and nucleic acid functional groups replacing the interactions of these functional groups otherwise provided by water (*1*, *3*, *73*). Analyses (*1*, *3*) of protein−nucleic acid structural studies illustrate that a large fraction of the hydrogen bonds spanning the binding interfaces of cognate complexes have donor−acceptor distances that are too short to accommodate bridging waters (< 3.5 Å). For example, Janin and co-workers reported that 98% of protein−nucleic acid donor−acceptor distances were shorter than 3.4 Å and 67% were shorter than 3.0 Å (*3*). Recently, the large stabilizing effect of glycine betaine on the equilibrium constant for specific binding of lac repressor to lac operator DNA has been quantitatively interpreted in terms of the loss of more than 1200 waters of hydration (and some glycine betaine) from almost 7000 Å^2 of repressor and operator surface buried in this interaction (*74*). (Burial of 630 Å^2 of DNA phosphate surface area, with release of approximately 170 waters of hydration from which glycine betaine was completely excluded in the uncomplexed DNA, was shown to contribute the majority of the stabilizing effect of glycine betaine.) More generally, effects of glycine betaine, urea, and Hofmeister salts on protein−DNA interactions, on protein folding, and other protein processes are explained in terms of the loss of approximately two layers of water from all surfaces buried in the interface (*74*−*77*).

Conversely, interfaces of nonspecific complexes of oligocations like KWKK and HWKK with nucleic acids probably are fully hydrated based on three lines of evidence. First, experimentally determined K_{obs} and SK_{obs} values for oligocation−nucleic acid binding processes were accurately predicted by Poisson−Boltzmann calculations which only account for Coulombic interactions and not changes in surface hydration (*78*). Second, oligopeptide−polyU binding constants were essentially indistinguishable as a function of anion composition at constant salt concentration (*4*). If significant dehydration occurred in these interactions, specific effects of different Hofmeister anions on the binding constant would be expected (*77*). Finally, NMR studies (*79*, *80*) demonstrated that polyamines bound to DNA are highly mobile, which is consistent with a hydrated, Coulombic, "loose" polyamine−DNA complex. Therefore, XWKK−RNA complexes most likely have hydrated binding interfaces which are exclusively stabilized by long-range Coulombic interactions. Our studies show that an addition of 1−2 positive charges on XWKK to increase Coulombic interactions across the hydrated interface is not sufficiently favorable to promote protonation of histidine or the α-amino group at a pH above their respective typical pK_a values. However, in the dehydrated interfaces of specifically bound complexes, residues interact directly instead of through water. Protein−nucleic acid binding processes exhibiting coupled histidine protonation require that histidine interact via the proton that makes it positively charged to satisfy the salt bridges or other necessary hydrogen bonds with the nucleic acid. In these cases, the free energy penalty of protonating histidine above its nominal pK_a is much less than the consequences of not fulfilling the interactions it provides. These findings provide a rationale explaining why the presence of histidine coupled protonation exhibited by some nucleic acid-binding proteins depends on the nucleic acid sequences to which they bind (*18*, *26*−*28*).

Site Size of XWKK Binding to polyU Is Invariant with pH and Larger than Predicted by Charge Neutralization Alone. Nonspecific binding of many cationic ligands to nucleic acids exhibits a site size approximately equal to the number of charges neutralized in the ligand−nucleic acid complex. Examples include inorganic salts such as Mg^{2+} (*6*, *47*) and $Co(NH_3)_6^{3+}$ (*31*), polyamines (*32*), and oligopeptides of varying lengths (*4*−*6*, *13*, *34*, *35*, *46*). A small ligand such as Mg^{2+} binding to polyU or poly(rA)−polyU has a site size $n = 2.0 \pm 0.1$ and $n = 2.2 \pm 0.1$ respectively (*47*), and KWK_6 bound to homopolymeric deoxythymidylate (polydT) ssDNA with $n \approx 8$ under stoichiometric binding conditions (*35*). However, the site sizes of KWKK and KWKK were larger than expected if a 1:1 correlation of charge to lattice occupation size is assumed. For both HWKK and KWKK, the site size was about 5 nucleotides both by nonlinear least-squares analysis of binding isotherms and via independent measurement of stoichiometric binding at low pH. In addition, we saw no obvious dependence on site size with protonation state, even for HWKK whose charge (Z_L) decreases from ~4 to ~2 over pH 5.2−8.7 (Table S1, Supporting Information).

Flexibility of the oligopeptide and/or nucleic acid may play a role in explaining these findings. Unstructured oligopeptides of intermediate length appear to have slightly larger site sizes when binding double-stranded DNA (dsDNA) than would be expected from ligand charge alone. Spermine (a polyamine with $Z_L = 4$) has an average site size of $n = 4.9 \pm 0.3$ phosphates at pH 6.5 between 71−132 mM Na^+ (*32*) and WK_4 ($Z_L = 4$) binds at 6.4 mM Na^+ pH 7.0 with $n = 4.6 \pm 0.5$ (*34*). Larger ligands of the form ε-DNP-Lys-$(Lys)_x$, where x indicates the number of unmodified lysines and the total charge Z_L, bind poly(rA)−polyU with $n = 6.6$ when $Z_L = 5$ and with $n = 7.1$ when $Z_L = 6$ (*9*, *30*). These results suggest that ligand conformational constraints may require a larger nucleic acid site size than expected based on charge neutralization alone. The converse of this phenomenon, where ligand flexibility permits interstitial residue compaction upon nucleic acid binding, was observed for a series of 17-residue $Z_L = 4$ oligopeptides each of which bound dsDNA with a comparable site size of $n = 4.0 \pm 0.7$ and most exhibited a concomitant conformational transition from random-coil to α-helix by circular dichroism (*34*). The pH invariant site size $n \approx 5$ for XWKK may be due to inherent inflexibility which prohibits decreases in site size as Z_L decreases.

To determine the dependence of nucleic acid binding as a function of peptide charge, nucleic acid base composition and salt effects, Lohman et al. estimated site size either by linear extrapolation of ν/L_F to $\nu/L_F = 0$ on a Scatchard plot (*4*) or assumed that site size was proportional to oligopeptide charge (*5*, *6*, *13*). Our results suggest that this assumption may not be justified for the shorter oligopeptides they considered. However, because the McGhee−von Hippel isotherm determines K_{obs} in the zero-binding density limit (i.e., as if a single ligand were binding at the center of an infinitely long lattice), site size effects are expected to be fairly inconsequential. Indeed, Mascotti and Lohman reported that increasing the site size ~20% resulted in only a 4% perturbation to log K_{obs} (*6*). Given the comparative approach of their studies and the relatively insensitive nature of the McGhee−von Hippel equilibrium binding constant to n, the discrepancy in site size does not impinge the major findings of these previous studies. Nevertheless, the larger site size has potential implications for complex formation with finite lattices at higher binding densities where ligands have to compete for overlapping sites.

In conclusion, our nonspecific binding studies of HWKK and KWKK to polyU reveal that protonated histidine and lysine have equivalent effects on the stability of these nucleic acid complexes and that reduction in the binding constant with increasing salt concentration is well-described by limiting-law polyelectrolyte theory. Both tetrapeptides, with a maximum of 4 positive charges, have a site size of ~5 nucleotides which does not vary significantly with pH or salt concentration. Binding constants for nonspecific interactions of HWKK and KWKK to polyU increase with protonation of histidine and the α-amino group, but pK_a shifts coupled to binding are not observed and there is no requirement for protonation. This contrasts with well-documented examples of histidine pK_a shifts and proton uptake in the binding of native proteins to nucleic acids. We propose that this disparity in histidine protonation behavior derives from differences in interface hydration. The interface in the nonspecific, Coulombically driven complexes of HWKK and KWKK with polyU is almost certainly fully hydrated, in contrast to the largely dehydrated, complementary interfaces of many native protein−nucleic acid complexes. We find that the additional Coulombic stabilization of a nonspecific HWKK−polyU complex provided by protonation is insufficient to cause a histidine pK_a shift and proton uptake upon binding. Conversely, the pK_a shifts and coupled protonation observed in several protein−nucleic acid binding processes (presumably) reflect the requirement for a salt bridge or other specific interaction with the protonated histidine in the significantly dehydrated binding interface.

SUPPORTING INFORMATION AVAILABLE

Data from additional control experiments referenced in the text. This material is available free of charge via the Internet at http://pubs.acs.org.

REFERENCES

1. Nadassy, K., Wodak, S. J., and Janin, J. (1999) Structural features of protein−nucleic acid recognition sites. *Biochemistry 38*, 1999–2017.
2. Honig, B., and Nicholls, A. (1995) Classical electrostatics in biology and chemistry. *Science 268*, 1144–1149.
3. Allers, J., and Shamoo, Y. (2001) Structure-based analysis of protein−RNA interactions using the program ENTANGLE. *J. Mol. Biol. 311*, 75–86.
4. Mascotti, D. P., and Lohman, T. M. (1990) Thermodynamic extent of counterion release upon binding oligolysines to single-stranded nucleic acids. *Proc. Natl. Acad. Sci. U.S.A. 87*, 3146.
5. Mascotti, D. P., and Lohman, T. M. (1993) Thermodynamics of single-stranded RNA and DNA interactions with oligolysines containing tryptophan. Effects of base composition. *Biochemistry 32*, 10568–10579.
6. Mascotti, D. P., and Lohman, T. M. (1992) Thermodynamics of single-stranded RNA binding to oligolysines containing tryptophan. *Biochemistry 31*, 8932–8946.
7. Lohman, T. M., deHaseth, P. L., and Record, M. T., Jr. (1980) Pentalysine−deoxyribonucleic acid interactions: a model for the general effects of ion concentrations on the interactions of proteins with nucleic acids. *Biochemistry 19*, 3522–3530.
8. Record, M. T., Jr., Lohman, T. M., and deHaseth, P. (1976) Ion effects on ligand-nucleic acid interactions. *J. Mol. Biol. 107*, 145–158.
9. Latt, S. A., and Sober, H. A. (1967) Protein−nucleic acid interactions. II. Oligopeptide−polyribonucleotide binding studies. *Biochemistry 6*, 3293–3306.
10. Latt, S. A., and Sober, H. A. (1967) Protein−nucleic acid interactions. III. Cation effect on binding strength and specificity. *Biochemistry 6*, 3307–3314.
11. Helene, C., and Maurizot, J. C. (1981) Interactions of oligopeptides with nucleic acids. *CRC Crit. Rev. Biochem. 10*, 213–258.
12. Helene, C., and Lancelot, G. (1982) Interactions between functional groups in protein−nucleic acids associations. *Prog. Biophys. Mol. Biol. 39*, 1–68.
13. Mascotti, D. P., and Lohman, T. M. (1997) Thermodynamics of oligoarginines binding to RNA and DNA. *Biochemistry 36*, 7272–7279.
14. Schultz, S. C., Shields, G. C., and Steitz, T. A. (1991) Crystal structure of a CAP−DNA complex—the DNA is bent by 90°. *Science 253*, 1001–1007.
15. Parkinson, G., Wilson, C., Gunasekera, A., Ebright, Y. W., Ebright, R. E., and Berman, H. M. (1996) Structure of the CAP−DNA complex at 2.5 Å resolution: A complete picture of the protein−DNA interface. *J. Mol. Biol. 260*, 395–408.
16. Muller, C. W., Rey, F. A., Sodeoka, M., Verdine, G. L., and Harrison, S. C. (1995) Structure of the NF-κB p50 homodimer bound to DNA. *Nature 373*, 311–317.
17. Doublie, S., Tabor, S., Long, A. M., Richardson, C. C., and Ellenberger, T. (1998) Crystal structure of a bacteriophage T7 DNA replication complex at 2.2 Å resolution. *Nature 391*, 251–258.
18. Luisi, B. F., Xu, W. X., Otwinowski, Z., Freedman, L. P., Yamamoto, K. R., and Sigler, P. B. (1991) Crystallographic analysis of the interaction of the glucocorticoid receptor with DNA. *Nature 352*, 497–505.
19. Aviv, T., Lin, Z., Ben-Ari, G., Smibert, C. A., and Sicheri, F. (2006) Sequence-specific recognition of RNA hairpins by the SAM domain of Vts1p. *Nat. Struct. Mol. Biol. 13*, 168–176.
20. Astatke, M., Grindley, N. D. F., and Joyce, C. M. (1995) Deoxynucleoside triphosphate and pyrophosphate binding-sites in the catalytically competent ternary complex for the polymerase reaction catalyzed by DNA-Polymerase-I (Klenow fragment). *J. Biol. Chem. 270*, 1945–1954.
21. Park, C., Schultz, L. W., and Raines, R. T. (2001) Contribution of the active site histidine residues of ribonuclease A to nucleic acid binding. *Biochemistry 40*, 4949–4956.
22. Kim, O. T. P., Yura, K., and Go, N. (2006) Amino acid residue doublet propensity in the protein−RNA interface and its application to RNA interface prediction. *Nucleic Acids Res. 34*, 6450–6460.
23. Luscombe, N. M., Laskowski, R. A., and Thornton, J. M. (2001) Amino acid−base interactions: a three-dimensional analysis of protein−DNA interactions at an atomic level. *Nucleic Acids Res. 29*, 2860–2874.
24. Harrison, J. G., and Balasubramanian, S. (1998) Synthesis and hybridization analysis of a small library of peptide−oligonucleotide conjugates. *Nucleic Acids Res. 26*, 3136–3145.
25. Lundback, T., van den Berg, S., and Hard, T. (2000) Sequence-specific DNA binding by the glucocorticoid receptor DNA-binding domain is linked to a salt-dependent histidine protonation. *Biochemistry 39*, 8909–8916.
26. deHaseth, P. L., Lohman, T. M., and Record, M. T., Jr. (1977) Nonspecific interaction of lac repressor with DNA: an association reaction driven by counterion release. *Biochemistry 16*, 4783–4790.
27. Bradshaw, E. M., Sanford, D. G., Luo, X., Sudmeier, J. L., Gurard-Levin, Z. A., Bullock, P. A., and Bachovchin, W. W. (2004) T antigen origin-binding domain of Simian Virus 40: determinants of specific DNA binding. *Biochemistry 43*, 6928–6936.
28. Eliseo, T., Sánchez, I. E., Nadra, A. D., Dellarole, M., Paci, M., de Prat Gay, G., and Cicero, D. O. (2009) Indirect DNA readout on the protein side: coupling between histidine protonation, global structural cooperativity, dynamics, and DNA binding of the human papillomavirus type 16 E2C domain. *J. Mol. Biol. 388*, 327–344.
29. Bergqvist, S., Williams, M. A., O'Brien, R., and Ladbury, J. E. (2004) Heat capacity effects of water molecules and ions at a protein−DNA interface. *J. Mol. Biol. 336*, 829–842.
30. McGhee, J. D., and von Hippel, P. H. (1974) Theoretical aspects of DNA−protein interactions: cooperative and non-cooperative binding of large ligands to a one-dimensional homogeneous lattice. *J. Mol. Biol. 86*, 469–489.
31. Plum, G. E., and Bloomfield, V. A. (1988) Equilibrium dialysis study of binding of hexammine cobalt(III) to DNA. *Biopolymers 27*, 1045–1051.
32. Braunlin, W. H., Strick, T. J., and Record, M. T., Jr. (1982) Equilibrium dialysis studies of polyamine binding to DNA. *Biopolymers 21*, 1301–1314.
33. Bujalowski, W., and Lohman, T. M. (1989) Negative cooperativity in *Escherichia coli* single strand binding protein−oligonucleotide interactions: I. Evidence and a quantitative model. *J. Mol. Biol. 207*, 249–268.
34. Padmanabhan, S., Zhang, W., Capp, M. W., Anderson, C. F., and Record, M. T., Jr. (1997) Binding of cationic (+4) alanine- and glycine-containing oligopeptides to double-stranded DNA: thermodynamic analysis of effects of Coulombic interactions and α-helix induction. *Biochemistry 36*, 5193–5206.
35. Zhang, W., Bond, J. P., Anderson, C. F., Lohman, T. M., and Record, M. T., Jr. (1996) Large electrostatic differences in the binding thermodynamics of a cationic peptide to oligomeric and polymeric DNA. *Proc. Natl. Acad. Sci. U.S.A. 93*, 2511–2516.
36. Record, M. T., Jr., Zhang, W., and Anderson, C. F. (1998) Analysis of effects of salts and uncharged solutes on protein and nucleic acid equilibria and processes: a practical guide to recognizing and interpreting polyelectrolyte effects, Hofmeister effects, and osmotic effects of salts. *Adv. Protein Chem. 51*, 281–353.
37. Epstein, I. R. (1978) Cooperative and non-cooperative binding of large ligands to a finite one-dimensional lattice. A model for ligand−oligonucleotide interactions. *Biophys. Chem. 8*, 327–339.
38. Ni, H. H., Anderson, C. F., and Record, M. T., Jr. (1999) Quantifying the thermodynamic consequences of cation (M^{2+}, M^{+}) accumulation and anion (X^{-}) exclusion in mixed salt solutions of polyanionic DNA using Monte Carlo and Poisson−Boltzmann calculations of ion−polyion preferential interaction coefficients. *J. Phys. Chem. B 103*, 3489–3504.
39. Rouzina, I., and Bloomfield, V. A. (1997) Competitive electrostatic binding of charged ligands to polyelectrolytes: Practical approach using the nonlinear Poisson−Boltzmann equation. *Biophys. Chem. 64*, 139–155.
40. Rouzina, I., and Bloomfield, V. A. (1996) Macroion attraction due to electrostatic correlation between screening counterions 0.1. Mobile surface-adsorbed ions and diffuse ion cloud. *J. Phys. Chem. 100*, 9977–9989.
41. Ray, J., and Manning, G. S. (1992) Theory of delocalized ionic binding to polynucleotides—structural and excluded-volume effects. *Biopolymers 32*, 541–549.
42. Lohman, T. M., and Mascotti, D. P. (1992) Nonspecific ligand−DNA equilibrium binding parameters determined by fluorescence methods. *Methods Enzymol. 212*, 424–458.
43. Overman, L. B., Bujalowski, W., and Lohman, T. M. (1988) Equilibrium binding of *Escherichia coli* single-strand binding protein to single-stranded nucleic-acids in the $(SSB)_{65}$ binding mode—cation and anion effects and polynucleotide specificity. *Biochemistry 27*, 456–471.

44. Anderson, C. F., and Record, M. T., Jr. (1995) Salt nucleic−acid interactions. *Annu. Rev. Phys. Chem. 46*, 657–700.
45. Anderson, C. F., and Record, M. T., Jr. (1993) Salt dependence of oligoion polyion binding—a thermodynamic description based on preferential interaction coefficients. *J. Phys. Chem. 97*, 7116–7126.
46. Zhang, W. T., Ni, H. H., Capp, M. W., Anderson, C. F., Lohman, T. M., and Record, M. T., Jr. (1999) The importance of Coulombic end effects: experimental characterization of the effects of oligonucleotide flanking charges on the strength and salt dependence of oligocation (L^{8+}) binding to single-stranded DNA oligomers. *Biophys. J. 76*, 1008–1017.
47. Record, M. T., Jr., Anderson, C. F., and Lohman, T. M. (1978) Thermodynamic analysis of ion effects on the binding and conformational equilibria of proteins and nucleic acids: the roles of ion association or release, screening, and ion effects on water activity. *Q. Rev. Biophys. 11*, 103–178.
48. Record, M. T., Jr., Ha, J. H., and Fisher, M. A. (1991) Analysis of equilibrium and kinetic measurements to determine thermodynamic origins of stability and specificity and mechanism of formation of site-specific complexes between proteins and helical DNA. *Methods Enzymol. 208*, 291–343.
49. Olmsted, M. C., Bond, J. P., Anderson, C. F., and Record, M. T., Jr. (1995) Grand canonical Monte Carlo molecular and thermodynamic predictions of ion effects on binding of an oligocation (L^{8+}) to the center of DNA oligomers. *Biophys. J. 68*, 634–647.
50. Anderson, C. F., and Record, M. T., Jr. (1980) The relationship between the Poisson−Boltzmann model and the condensation hypothesis: an analysis based on the low salt form of the Donnan coefficient. *Biophys. Chem. 11*, 353–360.
51. Manning, G. S. (1969) Limiting laws and counterion condensation in polyelectrolyte solutions I. Colligative properties. *J. Chem. Phys. 51*, 924–933.
52. Edelhoch, H. (1967) Spectroscopic determination of tryptophan and tyrosine in proteins. *Biochemistry 6*, 1948–1954.
53. Ballin, J. D., Shkel, I. A., and Record, M. T., Jr. (2004) Interactions of the KWK_6 cationic peptide with short nucleic acid oligomers: demonstration of large Coulombic end effects on binding at 0.1−0.2 M salt. *Nucleic Acids Res. 32*, 3271–3281.
54. Shkel, I. A., Ballin, J. D., and Record, M. T., Jr. (2006) Interactions of cationic ligands and proteins with small nucleic acids: analytic treatment of the large Coulombic end effect on binding free energy as a function of salt concentration. *Biochemistry 45*, 8411–8426.
55. Johnson, M. L., and Frasier, S. G. (1985) Nonlinear least-squares analysis. *Methods Enzymol. 117*, 301–342.
56. Motulsky, H. Christopoulos, A. (2003) *Fitting Models to Biological Data Using Linear and Nonlinear Regression. A Practical Guide to Curve Fitting*, GraphPad Software, Inc., San Diego, CA.
57. Hurvich, C. M., and Tsai, C. L. (1989) Regression and time series model selection in small samples. *Biometrika 76*, 297–307.
58. Bujalowski, W., and Lohman, T. M. (1987) A general method of analysis of ligand−macromolecule equilibria using a spectroscopic signal from the ligand to monitor binding. Application to *Escherichia coli* single-strand binding protein−nucleic acid interactions. *Biochemistry 26*, 3099–3106.
59. Bond, J. P., Anderson, C. F., and Record, M. T., Jr. (1994) Conformational transitions of duplex and triplex nucleic acid helices: thermodynamic analysis of effects of salt concentration on stability using preferential interaction coefficients. *Biophys. J. 67*, 825–836.
60. Kao, Y. H., Fitch, C. A., Bhattacharya, S., Sarkisian, C. J., Lecomte, J. T. J., and Garcia-Moreno E, B. (2000) Salt effects on ionization equilibria of histidines in myoglobin. *Biophys. J. 79*, 1637–1654.
61. Lee, K. K., Fitch, C. A., Lecomte, J. T. J., and Garcia-Moreno E, B. (2002) Electrostatic effects in highly charged proteins: salt sensitivity of pK_a values of histidines in Staphylococcal nuclease. *Biochemistry 41*, 5656–5667.
62. Shire, S., Hanania, G., and Gurd, F. (1975) Electrostatic effects in myoglobin. Application of the modified Tanford−Kirkwood theory to myoglobins from horse, California grey whale, harbor seal, and California sea lion. *Biochemistry 14*, 1352–1358.
63. Shire, S., Hanania, G., and Gurd, F. (1974) Electrostatic effects in myoglobin. Hydrogen ion equilibria in sperm whale ferrimyoglobin. *Biochemistry 13*, 2967–2974.
64. Ferreiro, D. U., Dellarole, M., Nadra, A. D., and de Prat-Gay, G. (2005) Free energy contributions to direct readout of a DNA sequence. *J. Biol. Chem. 280*, 32480–32484.
65. Dawson, R. M. C., Elliott, D. C., Elliot, W. H., Jones, K. M. (1995) Data for Biochemical Research, Oxford University Press, New York.
66. Barkley, M. D., Lewis, P. A., and Sullivan, G. E. (1981) Ion effects on the lac repressor−operator equilibrium. *Biochemistry 20*, 3842–3851.
67. Kalodimos, C. G., Biris, N., Bonvin, A. M. J. J., Levandoski, M. M., Guennuegues, M., Boelens, R., and Kaptein, R. (2004) Structure and flexibility adaptation in nonspecific and specific protein−DNA complexes. *Science 305*, 386–389.
68. Cicero, D. O., Nadra, A. D., Eliseo, T., Dellarole, M., Paci, M., and de Prat-Gay, G. (2006) Structural and thermodynamic basis for the enhanced transcriptional control by the human papillomavirus strain-16 E2 protein. *Biochemistry 45*, 6551–6560.
69. Winkler, F. K., Banner, D. W., Oefner, C., Tsernoglou, D., Brown, R. S., Heathman, S. P., Bryan, R. K., Martin, P. D., Petratos, K., and Wilson, K. S. (1993) The crystal structure of *Eco*RV endonuclease and of its complexes with cognate and noncognate DNA fragments. *EMBO J. 12*, 1781–1795.
70. Gewirth, D. T., and Sigler, P. B. (1995) The basis for half-site specificity explored through a noncognate steroid receptor−DNA complex. *Nat. Struct. Mol. Biol. 2*, 386–394.
71. Cave, J. W., Kremer, W., and Wemmer, D. E (2000) Backbone dynamics of sequence specific recognition and binding by the yeast *Pho4* bHLH domain probed by NMR. *Protein Sci. 9*, 2354–2365.
72. Gao, M., and Skolnick, J. (2009) From nonspecific DNA−protein encounter complexes to the prediction of DNA−protein interactions. *PLoS Comput. Biol. 5*, e1000341.
73. Woda, J., Schneider, B., Patel, K., Mistry, K., and Berman, H. M. (1998) An analysis of the relationship between hydration and protein−DNA interactions. *Biophys. J. 75*, 2170–2177.
74. Capp, M. W., Pegram, L. M., Saecker, R. M., Kratz, M., Riccardi, D., Wendorff, T., Cannon, J. G., and Record, M. T., Jr. (2009) Interactions of the osmolyte glycine betaine with molecular surfaces in water: thermodynamics, structural interpretation, and prediction of *m*-values. *Biochemistry 48*, 10372–10379.
75. Meulen, K. A. V., Saecker, R. M., and Record, M. T., Jr. (2008) Formation of a wrapped DNA−protein interface: experimental characterization and analysis of the large contributions of ions and water to the thermodynamics of binding IHF to H' DNA. *J. Mol. Biol. 377*, 9–27.
76. Kontur, W. S., Saecker, R. M., Davis, C. A., Capp, M. W., and Record, M. T., Jr. (2006) Solute probes of conformational changes in open complex (RP_o) formation by *Escherichia coli* RNA polymerase at the λP_R promoter: evidence for unmasking of the active site in the isomerization step and for large-scale coupled folding in the subsequent conversion to RP_o. *Biochemistry 45*, 2161–2177.
77. Pegram, L. M., and Record, M. T., Jr. (2008) Thermodynamic origin of Hofmeister ion effects. *J. Phys. Chem. B 112*, 9428–9436.
78. Stigter, D., and Dill, K. A. (1996) Binding of ionic ligands to polyelectrolytes. *Biophys. J. 71*, 2064–2074.
79. Srivenugopal, K., Wemmer, D., and Morris, D. (1987) Aggregation of DNA by analogs of spermidine; enzymatic and structural studies. *Nucleic Acids Res. 15*, 2563–2580.
80. Wemmer, D. E., Srivenugopal, K. S., Reid, B. R., and Morris, D. R. (1985) Nuclear magnetic resonance studies of polyamine binding to a defined DNA sequence. *J. Mol. Biol. 185*, 457–459.